

Lawrence Berkeley National Laboratory

LBL Publications

Title

Modal characteristics of structures considering dynamic soil-structure interaction effects

Permalink

<https://escholarship.org/uc/item/7sb6x0wc>

Authors

Papadopoulos, Manthos
Van Beeumen, Roel
François, Stijn
[et al.](#)

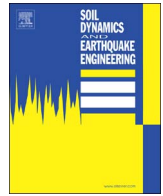
Publication Date

2018-02-01

DOI

10.1016/j.soildyn.2017.11.012

Peer reviewed



Modal characteristics of structures considering dynamic soil-structure interaction effects



Manthos Papadopoulos^{a,*}, Roel Van Beeumen^b, Stijn François^a, Geert Degrande^a, Geert Lombaert^a

^a KU Leuven, Department of Civil Engineering, Kasteelpark Arenberg 40, 3001 Leuven, Belgium

^b KU Leuven, Department of Computer Science, Celestijnenlaan 200A, B-3001 Leuven, Belgium

ARTICLE INFO

Keywords:

Dynamic soil-structure interaction
Perfectly matched layers
Modal characteristics of structures
Non-linear eigenvalue problem
Non-proportional damping

ABSTRACT

The modal characteristics of structures are usually computed disregarding any interaction with the soil. This paper presents a finite element-perfectly matched layers model to compute the modal characteristics of 2D and 3D coupled soil-structure systems while taking fully into account dynamic soil-structure interaction. The methodology can facilitate the interpretation of experimentally identified modal characteristics by assessing the importance of dynamic soil-structure interaction.

1. Introduction

The modal characteristics of structures are usually computed with finite element models disregarding any interaction with the soil. These modal characteristics can differ from the ones identified by means of experimental modal analysis [1]. Finite element updating is used to reduce the discrepancy between numerically predicted and experimentally identified modal characteristics by appropriately calibrating model parameters [2]. Dynamic soil-structure interaction (SSI) affects the modal characteristics due to the more flexible support conditions and the dissipation of energy in the soil [3]. Disregarding dynamic SSI might result in poor correspondence between numerical and experimental modal characteristics. Effects from dynamic SSI might be erroneously lumped to structural parameters during finite element updating, leading to model errors adversely affecting accurate prediction of structural vibration. Dynamic SSI can be accounted for by using coupled finite element-boundary element (FE-BE) formulations [4] or finite element formulations in conjunction with absorbing boundary conditions (ABC) [5] or perfectly matched layers (PML) [6]. In these models, the influence of the semi-infinite extent of the soil is explicitly taken into account by allowing the radiation of elastodynamic waves.

The computation of the modal characteristics of these coupled soil-structure models requires the solution of non-linear eigenvalue problems which are more challenging to solve than the generalized eigenvalue problem. This paper presents a FE-PML model facilitating the computation of the modal characteristics of 2D and 3D coupled soil-

structure systems. These results can support the interpretation of experimentally identified modal characteristics by quantifying the influence of dynamic SSI. Ultimately, the FE-PML model can be used in vibration based finite element updating where both soil and structural parameters are calibrated.

2. FE-PML model

Fig. 1 shows the FE-PML model used to compute the modal characteristics of coupled soil-structure systems. The structure Ω_b is partially embedded in a stratified soil Ω_s^c . The computational domain Ω is composed by the generalized structure $\Omega_r = \Omega_b \cup \Omega_s^c$ modeled with FE and the PML buffer zone Ω_p simulating the truncated unbounded soil at Σ_{rp} .

The virtual work equation for the generalized structure Ω_r in the frequency domain is:

$$\int_{\Omega_r} (\mathbf{L}\hat{\mathbf{v}})^T \mathbf{C} (\mathbf{L}\hat{\mathbf{u}}) d\Omega + (i\omega)^2 \int_{\Omega_r} \rho \hat{\mathbf{v}}^T \hat{\mathbf{u}} d\Omega = \int_{\Gamma^N} \hat{\mathbf{v}}^T \hat{\mathbf{t}}^n d\Gamma + \int_{\Sigma_{rp}} \hat{\mathbf{v}}^T \hat{\mathbf{t}}^n d\Gamma \quad (1)$$

where $\hat{\mathbf{u}}$ is the displacement vector, $\hat{\boldsymbol{\varepsilon}} = \{\hat{\varepsilon}_{xx}, \hat{\varepsilon}_{yy}, \hat{\varepsilon}_{zz}, \hat{\gamma}_{xy}, \hat{\gamma}_{yz}, \hat{\gamma}_{zx}\}^T = \mathbf{L}\hat{\mathbf{u}}$ is the strain vector, \mathbf{L} is a matrix containing differential operators, $\hat{\boldsymbol{\sigma}} = \{\hat{\sigma}_{xx}, \hat{\sigma}_{yy}, \hat{\sigma}_{zz}, \hat{\sigma}_{xy}, \hat{\sigma}_{yz}, \hat{\sigma}_{zx}\}^T = \mathbf{C}\hat{\boldsymbol{\varepsilon}}$ is the stress vector collecting the elements of the symmetric stress tensor σ_{ij} , \mathbf{C} is the constitutive matrix, ρ is the density, $\hat{\mathbf{t}}^n$ are applied tractions with \mathbf{n} the unit outward normal vector and $\hat{\mathbf{v}}$ is a kinematically admissible virtual displacement field on Ω . A hat above a variable denotes its representation in the frequency

* Corresponding author.

E-mail addresses: manthos.papadopoulos@kuleuven.be (M. Papadopoulos), roel.vanbeeumen@kuleuven.be (R. Van Beeumen), stijn.francois@kuleuven.be (S. François), geert.degrande@kuleuven.be (G. Degrande), geert.lombaert@kuleuven.be (G. Lombaert).

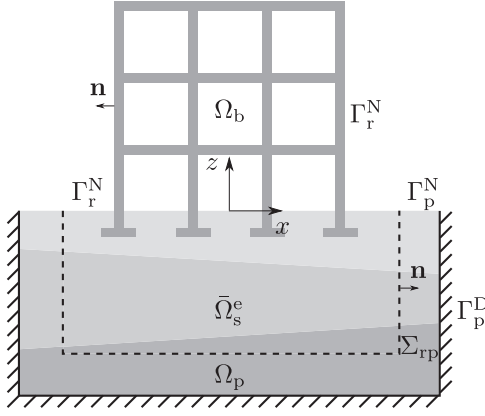


Fig. 1. FE-PML model.

domain. The last integral on the right hand-side is the interaction term on Σ_{rp} with the PML buffer zone Ω_p where the traction equilibrium $\hat{\mathbf{t}}_r^n + \hat{\mathbf{t}}_p^{-n} = \mathbf{0}$ holds.

Complex coordinate stretching is applied inside the PML buffer zone Ω_p in order to artificially attenuate the elastodynamic waves [6,7]. For a coordinate s , representing the x , y or z coordinate, the stretched coordinate \tilde{s} is defined as:

$$\tilde{s} = s_0 + \int_{s_0}^{s_1} \hat{\lambda}_s(s) ds = s_0 + \int_{s_0}^{s_1} \alpha_{0s}(s) ds + \frac{1}{i\omega} \int_{s_0}^{s_1} \alpha_{1s}(s) ds \quad (2)$$

where s_0 and s_1 delimit the origin and the termination of the PML buffer zone in the direction of the coordinate s and $\hat{\lambda}_s(s)$ is the stretch function with $\alpha_{0s}(s)$ and $\alpha_{1s}(s)$ polynomial functions controlling the attenuation of the evanescent and propagating waves inside the PML buffer zone [8]. Introducing the complex coordinate stretching (2), the equilibrium equation of the PML buffer zone Ω_p is:

$$(\hat{\lambda}_y \hat{\lambda}_z \mathbf{L}_x^T + \hat{\lambda}_x \hat{\lambda}_z \mathbf{L}_y^T + \hat{\lambda}_x \hat{\lambda}_y \mathbf{L}_z^T) \hat{\boldsymbol{\sigma}} = (i\omega)^2 \rho \hat{\lambda}_x \hat{\lambda}_y \hat{\lambda}_z \hat{\mathbf{u}} \quad \text{in } \Omega_p \quad (3)$$

where the differential operators \mathbf{L}_x , \mathbf{L}_y and \mathbf{L}_z are defined as:

$$\mathbf{L}_x = \begin{bmatrix} \frac{\partial}{\partial x} & 0 & 0 & 0 & 0 & 0 \\ 0 & 0 & 0 & \frac{\partial}{\partial x} & 0 & 0 \\ 0 & 0 & 0 & 0 & 0 & \frac{\partial}{\partial x} \end{bmatrix}^T$$

$$\mathbf{L}_y = \begin{bmatrix} 0 & 0 & 0 & \frac{\partial}{\partial y} & 0 & 0 \\ 0 & \frac{\partial}{\partial y} & 0 & 0 & 0 & 0 \\ 0 & 0 & 0 & 0 & \frac{\partial}{\partial y} & 0 \end{bmatrix}^T$$

$$\mathbf{L}_z = \begin{bmatrix} 0 & 0 & 0 & 0 & 0 & \frac{\partial}{\partial z} \\ 0 & 0 & 0 & 0 & \frac{\partial}{\partial z} & 0 \\ 0 & 0 & \frac{\partial}{\partial z} & 0 & 0 & 0 \end{bmatrix}^T \quad (4)$$

Similarly, the kinematic equation of the PML buffer zone in stretched coordinates, using $\hat{\boldsymbol{\varepsilon}} = \mathbf{D}\hat{\boldsymbol{\sigma}}$ with \mathbf{D} the compliance matrix, is:

$$\hat{\lambda}_x \hat{\lambda}_y \hat{\lambda}_z \mathbf{D} \hat{\boldsymbol{\sigma}} = (\hat{\lambda}_y \hat{\lambda}_z \mathbf{L}_x + \hat{\lambda}_x \hat{\lambda}_z \mathbf{L}_y + \hat{\lambda}_x \hat{\lambda}_y \mathbf{L}_z) \hat{\mathbf{u}} \quad \text{in } \Omega_p \quad (5)$$

The mixed formulation of Fathi et al. [9] is used for the modeling of the PML buffer zone Ω_p where both displacements and stresses are retained as independent variables. The equilibrium Eq. (3) and the kinematic Eq. (5) are treated independently. The integral form of the

equilibrium Eq. (3) is obtained by considering a kinematically admissible virtual displacement field $\hat{\mathbf{v}}$ on Ω , integrating by parts the terms depending on $\hat{\boldsymbol{\sigma}}$ and applying the divergence theorem:

$$\int_{\Omega_p} (\hat{\lambda}_y \hat{\lambda}_z \mathbf{L}_x \hat{\mathbf{v}} + \hat{\lambda}_x \hat{\lambda}_z \mathbf{L}_y \hat{\mathbf{v}} + \hat{\lambda}_x \hat{\lambda}_y \mathbf{L}_z \hat{\mathbf{v}})^T \hat{\boldsymbol{\sigma}} d\Omega + (i\omega)^2 \int_{\Omega_p} \rho \hat{\lambda}_x \hat{\lambda}_y \hat{\lambda}_z \hat{\mathbf{v}}^T \hat{\mathbf{u}} d\Omega = \int_{\Sigma_{rp}} \hat{\mathbf{v}}^T \hat{\mathbf{t}}^{-n} d\Gamma \quad (6)$$

where the integral on the right hand-side is the interaction term with the generalized structure Ω_r . The integral form of the kinematic Eq. (5) is obtained by considering a virtual stress field $\hat{\boldsymbol{\tau}}$ on Ω :

$$\int_{\Omega_p} \hat{\boldsymbol{\tau}}^T (\hat{\lambda}_y \hat{\lambda}_z \mathbf{L}_x + \hat{\lambda}_x \hat{\lambda}_z \mathbf{L}_y + \hat{\lambda}_x \hat{\lambda}_y \mathbf{L}_z) \hat{\mathbf{u}} d\Omega - \int_{\Omega_p} \hat{\lambda}_x \hat{\lambda}_y \hat{\lambda}_z \hat{\boldsymbol{\tau}}^T \mathbf{D} \hat{\boldsymbol{\sigma}} d\Omega = 0 \quad (7)$$

The dynamic SSI problem is formulated by taking into account the equilibrium of tractions on the interface Σ_{rp} . Adding Eqs. (1) and (6) yields:

$$\int_{\Omega_r} (\mathbf{L}\hat{\mathbf{v}})^T \mathbf{C}(\mathbf{L}\hat{\mathbf{u}}) d\Omega + (i\omega)^2 \int_{\Omega_r} \rho \hat{\mathbf{v}}^T \hat{\mathbf{u}} d\Omega + \int_{\Omega_p} (\hat{\lambda}_y \hat{\lambda}_z \mathbf{L}_x \hat{\mathbf{v}} + \hat{\lambda}_x \hat{\lambda}_z \mathbf{L}_y \hat{\mathbf{v}} + \hat{\lambda}_x \hat{\lambda}_y \mathbf{L}_z \hat{\mathbf{v}})^T \hat{\boldsymbol{\sigma}} d\Omega + (i\omega)^2 \int_{\Omega_p} \rho \hat{\lambda}_x \hat{\lambda}_y \hat{\lambda}_z \hat{\mathbf{v}}^T \hat{\mathbf{u}} d\Omega = \int_{\Gamma_r^N} \hat{\mathbf{v}}^T \hat{\mathbf{t}}^n d\Gamma \quad (8)$$

The combined integral Eqs. (7) and (8) describe the dynamic response of the coupled soil-structure system. A standard Galerkin procedure is followed in the FE implementation. The displacement field $\hat{\mathbf{u}}$ and the virtual displacement field $\hat{\mathbf{v}}$ are approximated as $\hat{\mathbf{u}} \approx \mathbf{N}_u \hat{\mathbf{u}}$ and $\hat{\mathbf{v}} \approx \mathbf{N}_v \hat{\mathbf{v}}$ with \mathbf{N}_u a matrix containing globally defined shape functions. Similarly, the stress field $\hat{\boldsymbol{\sigma}}$ and the virtual stress field $\hat{\boldsymbol{\tau}}$ are approximated as $\hat{\boldsymbol{\sigma}} \approx \mathbf{N}_\sigma \hat{\boldsymbol{\sigma}}$ and $\hat{\boldsymbol{\tau}} \approx \mathbf{N}_\tau \hat{\boldsymbol{\tau}}$. Since Eqs. (7) and (8) hold for any kinematically admissible virtual displacement field $\hat{\mathbf{v}}$ and virtual stress field $\hat{\boldsymbol{\tau}}$, the following system of equations is obtained:

$$\begin{bmatrix} \hat{\mathbf{S}}_{uu} & \hat{\mathbf{S}}_{u\sigma} \\ \hat{\mathbf{S}}_{u\sigma}^T & \hat{\mathbf{S}}_{\sigma\sigma} \end{bmatrix} \begin{bmatrix} \hat{\mathbf{u}} \\ \hat{\boldsymbol{\sigma}} \end{bmatrix} = \begin{bmatrix} \hat{\mathbf{p}} \\ \mathbf{0} \end{bmatrix} = \begin{bmatrix} \int_{\Gamma_r^N} \mathbf{N}_v^T \hat{\mathbf{t}}^n d\Gamma \\ \mathbf{0} \end{bmatrix} \quad (9)$$

where the block matrices are defined as follows:

$$\hat{\mathbf{S}}_{uu} = \int_{\Omega_r} (\mathbf{L}\mathbf{N}_u)^T \mathbf{C}(\mathbf{L}\mathbf{N}_u) d\Omega + (i\omega)^2 \int_{\Omega_r} \rho \mathbf{N}_u^T \mathbf{N}_u d\Omega + (i\omega)^2 \int_{\Omega_p} \rho \hat{\lambda}_x \hat{\lambda}_y \hat{\lambda}_z \mathbf{N}_u^T \mathbf{N}_u d\Omega \quad (10)$$

$$\hat{\mathbf{S}}_{u\sigma} = \int_{\Omega_p} (\hat{\lambda}_y \hat{\lambda}_z \mathbf{L}_x \mathbf{N}_u + \hat{\lambda}_x \hat{\lambda}_z \mathbf{L}_y \mathbf{N}_u + \hat{\lambda}_x \hat{\lambda}_y \mathbf{L}_z \mathbf{N}_u)^T \mathbf{N}_\sigma d\Omega \quad (11)$$

$$\hat{\mathbf{S}}_{\sigma\sigma} = - \int_{\Omega_p} \hat{\lambda}_x \hat{\lambda}_y \hat{\lambda}_z \mathbf{N}_\sigma^T \mathbf{D} \mathbf{N}_\sigma d\Omega \quad (12)$$

The system of Eqs. (9) is factorized into a rational form. In order to improve the conditioning of the system and preserve its symmetry, auxiliary stress variables $\hat{\boldsymbol{\xi}} = (i\omega\beta)^{-1} \hat{\boldsymbol{\sigma}}$ are introduced and the last row of the system is multiplied by $i\omega\beta$ where the scaling factor β depends on the stiffness and inertial parameters of the FE-PML model:

$$\begin{bmatrix} \hat{\mathbf{S}}_{uu} & i\omega\beta \hat{\mathbf{S}}_{u\sigma} \\ i\omega\beta \hat{\mathbf{S}}_{u\sigma}^T & (i\omega)^2 \beta^2 \hat{\mathbf{S}}_{\sigma\sigma} \end{bmatrix} \begin{bmatrix} \hat{\mathbf{u}} \\ \hat{\boldsymbol{\xi}} \end{bmatrix} = \begin{bmatrix} \hat{\mathbf{p}} \\ \mathbf{0} \end{bmatrix} \quad (13)$$

The polynomial products $i\omega\hat{\lambda}_y\hat{\lambda}_z$, $i\omega\hat{\lambda}_x\hat{\lambda}_z$, $i\omega\hat{\lambda}_x\hat{\lambda}_y$ and $(i\omega)^2\hat{\lambda}_x\hat{\lambda}_y\hat{\lambda}_z$ that now appear in Eq. (13) can be written as:

$$i\omega\hat{\lambda}_y\hat{\lambda}_z = (i\omega)^{-1} \alpha_{1y} \alpha_{1z} + \alpha_{0y} \alpha_{1z} + \alpha_{1y} \alpha_{0z} + i\omega \alpha_{0y} \alpha_{0z} = (i\omega)^{-1} d_{-1} + d_0 + i\omega d_1 \quad (14)$$

$$i\omega\hat{\lambda}_x\hat{\lambda}_z = (i\omega)^{-1} \alpha_{1x} \alpha_{1z} + \alpha_{0x} \alpha_{1z} + \alpha_{1x} \alpha_{0z} + i\omega \alpha_{0x} \alpha_{0z} = (i\omega)^{-1} f_{-1} + f_0 + i\omega f_1 \quad (15)$$

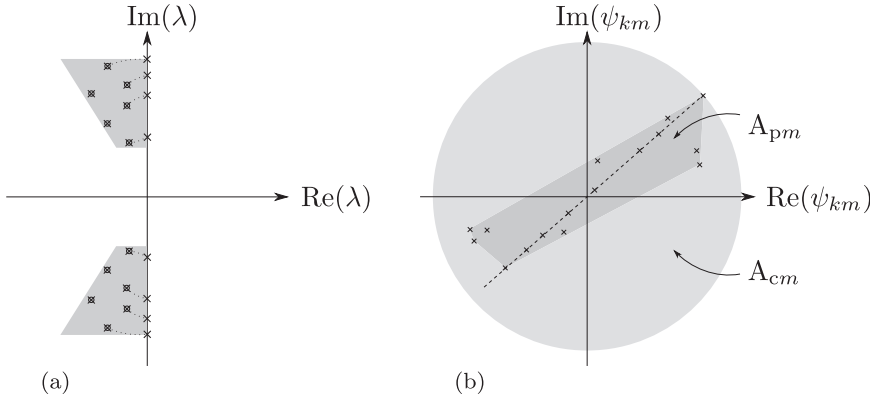


Fig. 2. (a) The eigensolver searches for eigenvalues (○) of the coupled soil-structure system in the neighborhood of the fixed base structure eigenfrequencies $i\omega_{rs}$ (×). (b) Definition of the MCF in Eq. (29). The × marks correspond to the modal displacements ψ_{km} of the superstructure. When a mode shape ψ_m is (virtually) real, all the elements ψ_{km} are located on a line.

$$i\omega\hat{\lambda}_x\hat{\lambda}_y = (i\omega)^{-1}\alpha_{1x}\alpha_{1y} + \alpha_{0x}\alpha_{1y} + \alpha_{1x}\alpha_{0y} + i\omega\alpha_{0x}\alpha_{0y} \\ = (i\omega)^{-1}g_{-1} + g_0 + i\omega g_1 \quad (16)$$

$$(i\omega)^2\hat{\lambda}_x\hat{\lambda}_y\hat{\lambda}_z = (i\omega)^{-1}\alpha_{1x}\alpha_{1y}\alpha_{1z} + \alpha_{0x}\alpha_{1y}\alpha_{1z} + \alpha_{1x}\alpha_{0y}\alpha_{1z} \\ + \alpha_{1x}\alpha_{1y}\alpha_{0z} + i\omega(\alpha_{0x}\alpha_{0y}\alpha_{1z} + \alpha_{0x}\alpha_{1y}\alpha_{0z} + \alpha_{1x}\alpha_{0y}\alpha_{0z}) \\ + (i\omega)^2\alpha_{0x}\alpha_{0y}\alpha_{0z} = (i\omega)^{-1}c_{-1} + c_0 + i\omega c_1 + (i\omega)^2c_2 \quad (17)$$

Using Eqs. (10)–(12) and (14)–(17), the system of equations (13) is factorized as:

$$\left(\frac{1}{i\omega} \begin{bmatrix} \mathbf{K}_{uu,-1} & \mathbf{K}_{us,-1} \\ \mathbf{K}_{us,-1}^T & \mathbf{K}_{ss,-1} \end{bmatrix} + \begin{bmatrix} \mathbf{K}_{uu,0} & \mathbf{K}_{us,0} \\ \mathbf{K}_{us,0}^T & \mathbf{K}_{ss,0} \end{bmatrix} \right) \\ + i\omega \begin{bmatrix} \mathbf{K}_{uu,1} & \mathbf{K}_{us,1} \\ \mathbf{K}_{us,1}^T & \mathbf{K}_{ss,1} \end{bmatrix} + (i\omega)^2 \begin{bmatrix} \mathbf{M}_{uu} & \mathbf{0} \\ \mathbf{0} & \mathbf{K}_{ss,2} \end{bmatrix} \begin{bmatrix} \hat{\mathbf{u}} \\ \hat{\mathbf{s}} \end{bmatrix} = \begin{bmatrix} \hat{\mathbf{p}} \\ \mathbf{0} \end{bmatrix} \quad (18)$$

where the block matrices are defined as follows:

$$\mathbf{M}_{uu} = \int_{\Omega_r} \rho \mathbf{N}_u^T \mathbf{N}_u d\Omega + \int_{\Omega_p} c_2 \rho \mathbf{N}_u^T \mathbf{N}_u d\Omega \quad (19)$$

$$\mathbf{K}_{uu,0} = \int_{\Omega_r} (\mathbf{L}\mathbf{N}_u)^T \mathbf{C} (\mathbf{L}\mathbf{N}_u) d\Omega + \int_{\Omega_p} c_0 \rho \mathbf{N}_u^T \mathbf{N}_u d\Omega \quad (20)$$

$$\mathbf{K}_{uu,j} = \int_{\Omega_p} c_j \rho \mathbf{N}_u^T \mathbf{N}_u d\Omega \quad (j = -1, 1) \quad (21)$$

$$\mathbf{K}_{us,j} = \beta \int_{\Omega_p} (d_j \mathbf{L}_x \mathbf{N}_u + f_j \mathbf{L}_y \mathbf{N}_u + g_j \mathbf{L}_z \mathbf{N}_u)^T \mathbf{N}_\sigma d\Omega \\ (j = -1, 0, 1) \quad (22)$$

$$\mathbf{K}_{ss,j} = -\beta^2 \int_{\Omega_p} c_j \mathbf{N}_\sigma^T \mathbf{D} \mathbf{N}_\sigma d\Omega \quad (j = -1, 0, 1, 2) \quad (23)$$

Although the FE-PML formulation is rather involved, the final form of the system matrices (19)–(23) is simple and can be easily implemented in existing finite element codes with minimum intervention. The system of Eqs. (18) corresponds to the following rational form:

$$\left[\frac{1}{i\omega} \tilde{\mathbf{D}} + \tilde{\mathbf{K}} + i\omega \tilde{\mathbf{C}} + (i\omega)^2 \tilde{\mathbf{M}} \right] \hat{\mathbf{u}} = \hat{\mathbf{f}} \quad (24)$$

For 2D problems in the kl -plane the polynomial products of $i\omega\hat{\lambda}_k$, $i\omega\hat{\lambda}_l$ and $(i\omega)^2\hat{\lambda}_k\hat{\lambda}_l$ in Eq. (13) are quadratic and the matrix $\tilde{\mathbf{D}}$ drops from the system of equations. In this case, Eqs. (21)–(23) apply for $j \geq 0$ with the stretch function parameters α_{0s} and α_{1s} of the non-active coordinate s equal to one.

3. Solution of the eigenvalue problem

The modal characteristics of the coupled soil-structure system are obtained by solving the rational eigenproblem:

$$\left[\frac{1}{\lambda_m} \tilde{\mathbf{D}} + \tilde{\mathbf{K}} + \lambda_m \tilde{\mathbf{C}} + \lambda_m^2 \tilde{\mathbf{M}} \right] \psi_m = \mathbf{0} \quad (25)$$

where $\lambda_m \in \mathbb{C}$ and $\psi_m \in \mathbb{C}^n$ ($m = 1, \dots, 3n$) with n the number of degrees of freedom in the FE-PML model. In the 2D case, the rational eigenproblem (25) simplifies to a quadratic eigenproblem with $\psi_m \in \mathbb{C}^n$ ($m = 1, \dots, 2n$).

The eigenproblem (25) is transformed into a larger linear matrix pencil which has the same eigenvalues as the original problem. Eq. (25) can be related to the generalized eigenvalue problem by defining the auxiliary vectors $\chi_{1m} = \lambda_m \psi_m$, $\chi_{2m} = \psi_m$ and $\chi_{3m} = \psi_m / \lambda_m$. Rearranging Eq. (25) and using these auxiliary vectors, the following linear matrix pencil $\mathbf{R}(\lambda)$ can be used [10]:

$$\mathbf{R}(\lambda_m) \tilde{\psi}_m = (\mathbf{A} - \lambda_m \mathbf{B}) \tilde{\psi}_m \\ = \left(\begin{bmatrix} -\tilde{\mathbf{C}} & -\tilde{\mathbf{K}} & -\tilde{\mathbf{D}} \\ \mathbf{I} & \mathbf{0} & \mathbf{0} \\ \mathbf{0} & \mathbf{I} & \mathbf{0} \end{bmatrix} - \lambda_m \begin{bmatrix} \tilde{\mathbf{M}} & \mathbf{0} & \mathbf{0} \\ \mathbf{0} & \mathbf{I} & \mathbf{0} \\ \mathbf{0} & \mathbf{0} & \mathbf{I} \end{bmatrix} \right) \tilde{\psi}_m = \mathbf{0} \quad (26)$$

where $\lambda_m \in \mathbb{C}$ and $\tilde{\psi}_m^T = \{\chi_{1m}^T, \chi_{2m}^T, \chi_{3m}^T\} = \{\lambda_m \psi_m^T, \psi_m^T, \psi_m^T / \lambda_m\} \in \mathbb{C}^{3n}$. In a similar way, defining the auxiliary vectors $\chi_{1m} = \psi_m$ and $\chi_{2m} = \lambda_m \psi_m$, the following linear matrix pencil $\mathbf{Q}(\lambda)$ can be used in the 2D case [11]:

$$\mathbf{Q}(\lambda_m) \tilde{\psi}_m = (\mathbf{A} - \lambda_m \mathbf{B}) \tilde{\psi}_m = \left(\begin{bmatrix} \tilde{\mathbf{K}} & \mathbf{0} \\ \mathbf{0} & \mathbf{I} \end{bmatrix} - \lambda_m \begin{bmatrix} -\tilde{\mathbf{C}} & -\tilde{\mathbf{M}} \\ \mathbf{I} & \mathbf{0} \end{bmatrix} \right) \tilde{\psi}_m = \mathbf{0} \quad (27)$$

where $\lambda_m \in \mathbb{C}$ and $\tilde{\psi}_m^T = \{\chi_{1m}^T, \chi_{2m}^T\} = \{\psi_m^T, \lambda_m \psi_m^T\} \in \mathbb{C}^{2n}$.

A compact rational Krylov (CoRK) eigensolver is used [12]. This eigensolver exploits the Kronecker structure below the first block row of the linearization pencils (26) and (27) and involves only matrix and vector operations of the original non-linear dimension n instead of $3n$ for (26) and $2n$ for (27) [13]. In the case of large-scale problems, the extra memory and orthogonalization cost due to the linearization of the original eigenproblem becomes negligible. Since only a subset of the eigenpairs (λ_m, ψ_m) of the coupled soil-structure system is usually of interest, the search of eigenvalues can be limited to the neighborhood of a few fixed base structure eigenfrequencies ω_{rs} (Fig. 2a).

The eigenpairs (λ_m, ψ_m) might correspond to modes of the coupled soil-structure system or non-physical modes of the PML. The real part of the eigenvalues λ_m is always negative for modes of the coupled soil-structure system ensuring that energy can only be dissipated within the system. These modes can be sorted into modes of the superstructure which tend to have small to moderate damping and modes of the generalized structure which generally are heavily damped. The former modes are of interest. The non-physical modes of the PML might have eigenvalues with positive real part. These are related to the stability issue of most PML formulations in the time domain. The cut-off frequency of these modes depends on the PML stretch function formulation. In order to assure that these modes lie well outside the frequency range of interest, the PML formulation can be verified by computing the fundamental solutions of the soil $\tilde{\Omega}_s^c$ in the frequency range of interest and examining their agreement with known solutions [14].

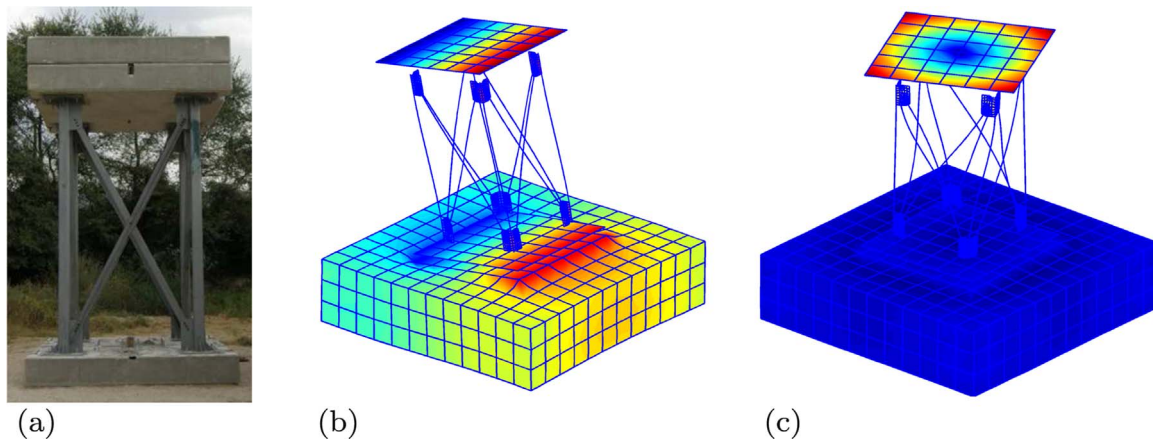


Fig. 3. (a) The Europroteas test structure [18]. (b) First lateral mode shape ψ_1 . (c) First torsional mode shape ψ_2 .

The eigenpairs (λ_m, ψ_m) occur in complex conjugate pairs for real-valued matrices $\tilde{\mathbf{D}}$, $\tilde{\mathbf{K}}$, $\tilde{\mathbf{C}}$ and $\tilde{\mathbf{M}}$ (i.e. systems without hysteretic damping) and undamped modes. The eigenfrequencies $\omega_{rm} \in \mathbb{R}$ and modal damping ratios $\xi_m \in \mathbb{R}$ are computed from the corresponding eigenvalues as:

$$\omega_{rm} = |\lambda_m| \quad \text{and} \quad \xi_m = -\frac{\text{Re}(\lambda_m)}{|\lambda_m|} \quad (28)$$

Fig. 2b shows how the phase coherence of a complex-valued mode shape ψ_m can be quantified by using the modal collinearity factor (MCF) [15]:

$$\text{MCF}_m = 1 - \frac{A_{pm}}{A_{cm}} \quad (29)$$

where A_{cm} is the circular area in the complex plane that is defined by the modal displacement ψ_{km} of the superstructure with the largest magnitude and A_{pm} is the convex area in the complex plane that enfolds all the modal displacements ψ_{km} of the superstructure. The MCF takes values from 0 to 1 with a value close to 1 indicating a (virtually) real mode.

4. Example

The methodology is demonstrated by computing the modal characteristics of the Europroteas test structure (Fig. 3a) which was specifically designed to study dynamic SSI [16]. The structure is assumed to rest at the surface of a halfspace with shear wave velocity $C_s = 130$ m/s, Poisson's ratio $\nu = 0.43$ and density $\rho = 2050$ kg/m³. The eigenfrequencies of the first lateral and torsional mode of the undamped fixed base model of the structure are $f_{s1} = 9.42$ Hz and $f_{s2} = 12.66$ Hz, respectively. The modal characteristics of the Europroteas test structure are affected by dynamic SSI with eigenfrequency shifting to significantly lower values and increased modal damping due to the radiation of elastodynamic waves in the soil. The corresponding eigenfrequencies and modal damping ratios considering dynamic SSI are $f_{r1} = 5.19$ Hz, $\xi_1 = 0.021$ and $f_{r2} = 11.53$ Hz, $\xi_2 = 0.031$. Figs. 3b and c show the related mode shapes ψ_1 and ψ_2 with $\text{MCF}_1 = 0.99$ and $\text{MCF}_2 = 0.98$, which indicate virtually real modes. The experimentally identified eigenfrequencies and (total) modal damping ratios are $f_{r1}^* = 4.1 - 4.3$ Hz, $\xi_1^{1*} = 0.030 - 0.034$ for the two lateral modes and $f_{r2}^* = 9.67$ Hz, $\xi_2^{1*} = 0.008$ for the torsional mode [17]. The numerically predicted modal characteristics f_{rm} and ξ_m do not match perfectly the experimentally identified ones f_{rm}^* and ξ_m^{1*} . However, they are a significant improvement when compared to the modal characteristics of the fixed base model. If dynamic SSI is disregarded in finite element updating, its effects will be eventually lumped to structural parameters, adversely affecting the accuracy of the updated model. The modal

characteristics of the Europroteas test structure considering dynamic SSI can be employed in vibration based finite element updating where both soil and structural parameters are updated.

5. Conclusions

This paper presents a FE-PML model to compute the modal characteristics of 2D and 3D coupled soil-structure systems. The model is developed using a mixed formulation for the PML where both displacements and stresses are retained as independent variables. The resulting eigenproblem, which has a rational form in 3D problems and a quadratic form in 2D problems, is solved using a compact rational Krylov eigensolver. The FE-PML model can be used to assess the influence of dynamic SSI on experimentally identified modal characteristics with potential application in vibration based finite element updating where both soil and structural parameters are calibrated.

Acknowledgments

This research was performed within the frame of the project OT/13/59 "Quantifying and reducing uncertainty in structural dynamics" funded by the Research Council of KU Leuven. The second author was supported by the project PDM/15/139 of the KU Leuven Research Council. The financial support is gratefully acknowledged. We would also like to thank Prof. Dimitris Pitilakis from Aristotle University of Thessaloniki for providing information on the Europroteas test structure.

References

- [1] Reynnders E. System identification methods for (operational) modal analysis: review and comparison. *Comput Methods Eng* 2012;19(1):51–124.
- [2] Simoen E, De Roeck G, Lombaert G. Dealing with uncertainty in model updating for damage assessment: a review. *Mech Syst Signal Process* 2015;56–57:123–49.
- [3] Beskos D, Krauthammer T, Vardoulakis I. Dynamic soil-structure interaction. A.A. Balkema; 1984.
- [4] Von Estorff O, Kausel E. Coupling of boundary and finite-elements for soil-structure interaction problems. *Earthq Eng Struct Dyn* 1989;18(7):1065–75.
- [5] Lysmer J, Kuhlemeyer R. Finite dynamic model for infinite media. *J Eng Mech Div* 1969;95(EM4):859–77.
- [6] Chew W, Liu Q. Perfectly matched layers for elastodynamics: a new absorbing boundary condition. *J Comput Acoust* 1996;4(4):341–59.
- [7] Chew W, Jin J, Michielssen E. Complex coordinate stretching as a generalized absorbing boundary condition. *Microw Opt Technol Lett* 1997;15(6):363–9.
- [8] Kucukcoban S, Kallivokas L. A symmetric hybrid formulation for transient wave simulations in PML-truncated heterogeneous media. *Wave Motion* 2013;50:57–79.
- [9] Fathi A, Poursartip B, Kallivokas L. Time-domain hybrid formulations for wave simulations in three-dimensional PML-truncated heterogeneous media. *Int J Numer Methods Eng* 2015;101:165–98.
- [10] Su Y, Bai Z. Solving rational eigenvalue problems via linearization. *SIAM J Matrix Anal Appl* 2011;32:201–16.
- [11] Tisseur F, Meerbergen K. The quadratic eigenvalue problem. *SIAM Rev* 2001;43:235–86.

- [12] CORK for solving nonlinear eigenvalue problems; August 2016. <<http://twr.cs.kuleuven.be/research/software/nleps/cork.php>>.
- [13] Van Beeumen R, Meerbergen K, Michiels W. Compact rational Krylov methods for nonlinear eigenvalue problems. *SIAM J Matrix Anal Appl* 2015;36(2):820–38.
- [14] Kausel E. *Fundamental solutions in elastodynamics: a compendium*. Cambridge University Press; 2006.
- [15] Ewins D. *Modal testing: theory, practice and applications*. Baldock, Hertfordshire, England: Research Studies Press Ltd; 2000.
- [16] Ptilakis D, Rovithis E, Massimino M, Gatto M. Numerical simulation of large-scale soil-foundation-structure interaction experiments in The EuroProteas facility. In: *Proceedings of the 6th international conference on earthquake geotechnical engineering*. Christchurch, New Zealand; 2015, p. 401.
- [17] Ptilakis D, Lamprou D, Manakou M, Rovithis E. System identification of soil-foundation structure systems by means of ambient noise records: the case of EuroProteas model structure in Euroseistest. In: *Proceedings of the 2nd European conference on earthquake engineering and seismology*. Istanbul, Turkey; 2014. p. 4337–47.
- [18] EUROSEISTEST database; February 2017. <<http://euroseisdb.civil.auth.gr/sfsis>>.